Supporting information

One-pot spatial engineering of multi-enzymes in metal-organic frameworks for enhanced cascade activity

Wenqing Fan[a], Kang Liang[a,b*], Jieying Liang,[a*]

[a]School of Chemical Engineering, Australian Centre for NanoMedicine, The University of New South Wales, Sydney, NSW 2052, Australia

[b]Graduate School of Biomedical Engineering, The University of New South Wales, Sydney, NSW 2052, Australia

Email: kang.liang@unsw.edu.au, jieying.liang@unsw.edu.au

1. Tables and Figures

Table S1 Enzyme loading efficiency of biocomposites.

GOx/HRP model	**GOx loading efficiency (%)**	**HRP loading efficiency (%)**
GOx/HRP-PDADMAC@ZIF-8	6.0±0.80	43.6±2.34
GOx-PDADMAC/HRP@ZIF-8	9.0±0.04	30.4±0.43
GOx/HRP@ZIF-8	6.8±0.34	40.4±1.72
GOx-PDADMAC/HRP-PDADMAC@ZIF-8	8.69±0.08	36.40±0.32
Pro/GOx model	**GOx loading efficiency (%)**	**Pro loading efficiency (%)**
Pro/GOx-PDADMAC@ZIF-8	5.85±0.80	13.69±0.80
Pro-PDADMAC/GOx@ZIF-8	3.30±0.19	13.50±0.79
Pro/GOx@ZIF-8	6.15±0.10	24.30±1.60
Pro/ADH model	**Pro loading efficiency(%)**	**ADH loading efficiency(%)**
Pro/ADH-PDADMAC@ZIF-8	14.25±0.8	18.75±0.98
Pro-PDADMAC/ADH@ZIF-8	14.40±0.53	17.40±1.90
Pro/ADH@ZIF-8	10.80±0.20	18.15±0.20

Table S2 The catalytic kinetic parameters of enzyme-MOF.

Biocomposites	**K_m (mM)**	**V_{max} (μM/min)**	**K ($min^{-1}\times10^{-5}$) (V_{max}/ K_m）**	**$K_{enzyme\text{-}MOF}/K_{free\ enzyme}$ (Times)**	**Relative activity (Times)**
GOx/HRP model					
GOx-PDADMAC/HRP@ZIF-8	1802.00	22.31	1.24	0.27	1.72
GOx-PDADMAC/HRP	915.70	41.80	4.56		
GOx/HRP-PDADMAC@ZIF-8	1754.00	18.82	1.07	0.22	1.38
GOx/HRP-PDADMAC	1018.00	50.25	4.94		
GOx/HRP@ZIF-8	275.90	2.451	0.89	0.16	1.00
GOx/HRP	784.60	44.12	5.62		
Pro/GOx model					
Pro-PDADMAC/GOx@ZIF-8	38.63	2.21	5.72	1.14	1.69
Pro-PDADMAC/GOx	23.69	1.19	5.03		
Pro/GOx-PDADMAC@ZIF-8	22.44	1.13	5.02	1.01	1.50
Pro/GOx-PDADMAC	26.77	1.33	4.96		
Pro/GOx@ZIF-8	31.33	1.24	3.97	0.68	1.00
Pro/GOx	25.25	1.48	5.86		
Pro/ADH model					
Pro/ADH-PDADMAC@ZIF-8	23.57	35.88	152.23	3.99	14.85
Pro/ADH-PDADMAC	24.34	9.29	38.20		
Pro-PDADMAC/ADH@ZIF-8	31.60	5.94	18.80	0.44	1.62
Pro-PDADMAC/ADH	23.76	10.26	43.24		
Pro/ADH@ZIF-8	23.95	3.23	13.54	0.27	1.00
Pro/ADH	23.82	11.96	50.23		

Table S3 Proportional peak area summary of deconvoluted amide I region in enzyme-MOF versus free enzymes.

Biocomposites	α-helix (%)	β-sheet (%)	intermolecular β-sheet (%)	β-turn (%)	random coil (%)
GOx/HRP	31.12	7.95	6.58	15.11	39.24
GOx-PDADMAC/HRP	31.23	17.10	13.75	11.48	26.45
GOx/HRP@ZIF-8	45.04	6.05	6.71	24.22	17.98
GOx-PDADMAC/HRP@ZIF-8	26.13	7.07	7.01	33.94	25.84
GOx/HRP-PDADMAC@ZIF-8	31.42	8.86	24.11	27.90	7.70

Table S4 Comparison of this work to other reported methods.

MOF	Enzymes	Method	Enhanced activity	Ref.
ZIF-8	GOx, HRP, Pro, ADH	PDADMAC-modified enzyme induced core-shell structure	1.69-14.85 times compared to unmodified bi-enzyme@ZIF-8.	This work
ZIF-8	GOx, HRP, Pro, ADH	Stepwise encapsulation of GOx and HRP by epitaxial shell-by-shell overgrowth	0.9-15.4 times compared to GOx/HRP@ZIF-8 and Pro/ADH/NAD^+@ZIF-8.	2
ZIF-8	GOx, HRP, β-galactosidase	Peptide-induced MOF super-self-assembly	4.4-7.3 times compared with the unassembled enzyme-MOF.	3
ZIF-8	GOx, HRP	Microfluidic techniques	About 3 times compared with the bulk solution–synthesized enzyme-MOF composites.	4
ZIF-8	GOx, Hemin	Dual confinement	1.7 times compared to the GOx/Hemin@ZIF.	5
ZIF-L	GOx, HRP, cofactor-dependent enzyme	Hollow MOF via tannic acid etching	Up to 16-fold higher enzymatic activity than the pristine biocatalytic MOFs	6

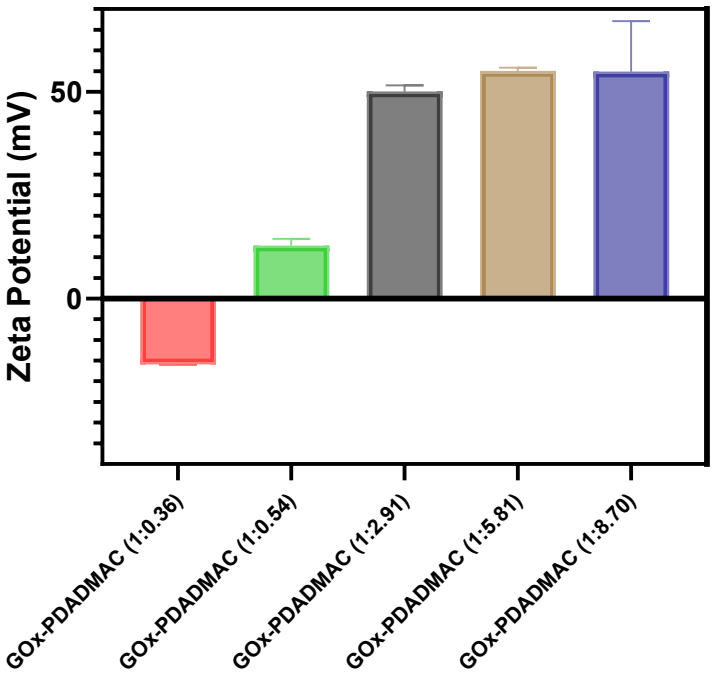

Figure S1. Zeta potential analysis of GOx modified with PDADMAC at various molar ratios.

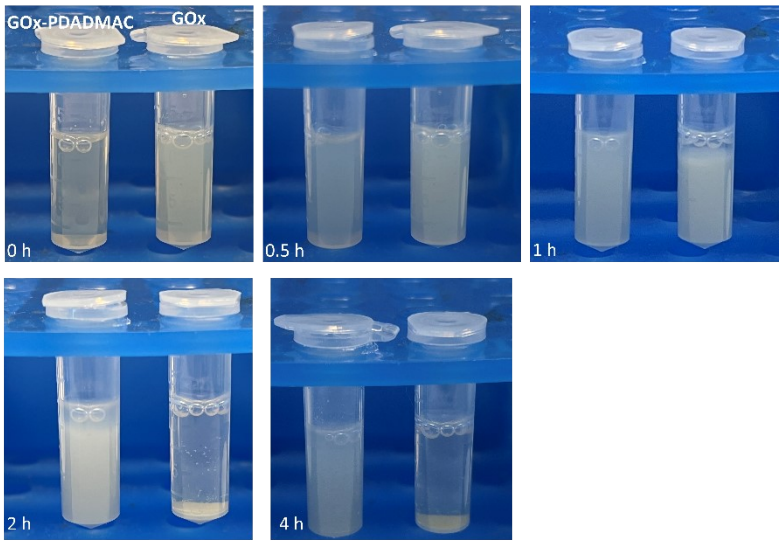

Figure S2. Synthesis progress of GOx-PDADMAC/HRP@ZIF-8 (left tube) and GOx/HRP@ZIF-8 (right tube).

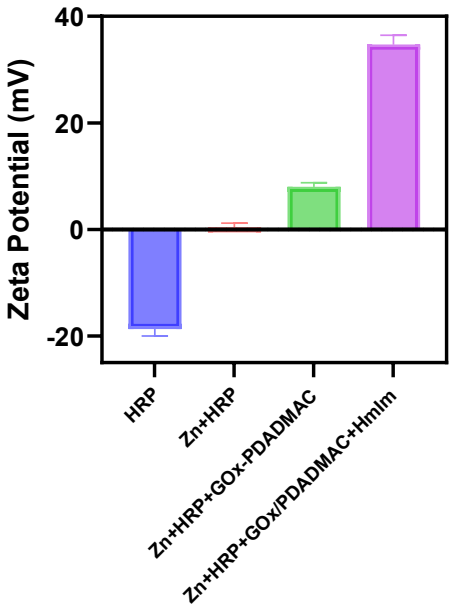

Figure S3. Zeta potential change during the synthesis of GOx-PDADMAC/HRP@ZIF-8 with the sequential addition of reagents.

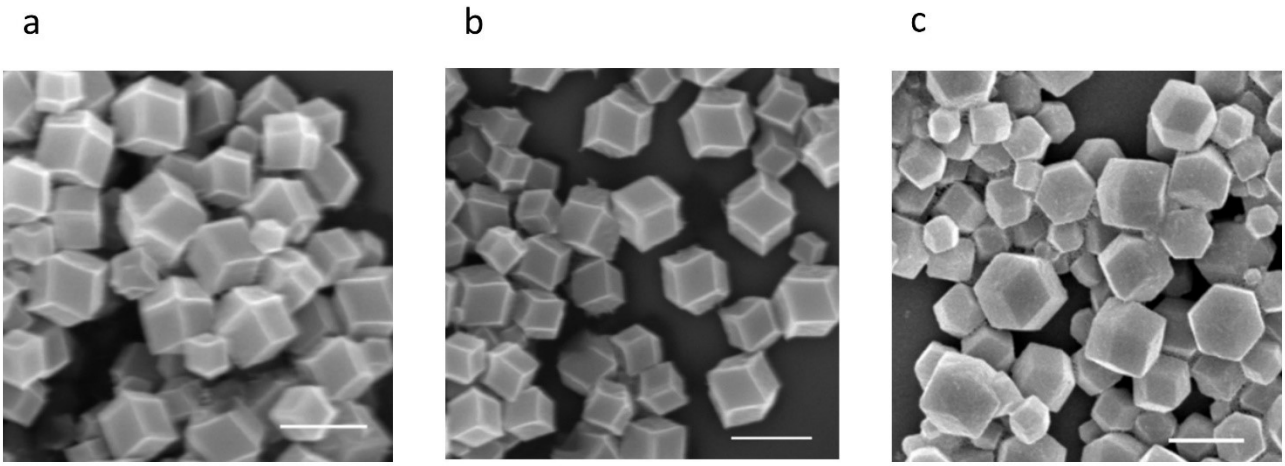

Figure S4. SEM images of as-synthesized GOx/HRP-PDADMAC@ZIF-8 **(a)**, GOx-PDADMAC/HRP@ZIF-8 **(b)**, GOx/HRP@ZIF-8 **(c).** The scale bar in the main images is 1 μm.

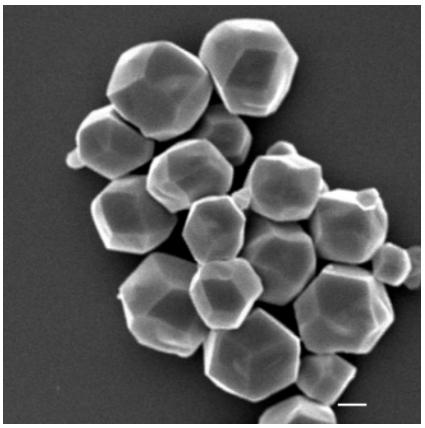

Figure S5. SEM images of ZIF-8. The scale bar in the main images is 1 μm.

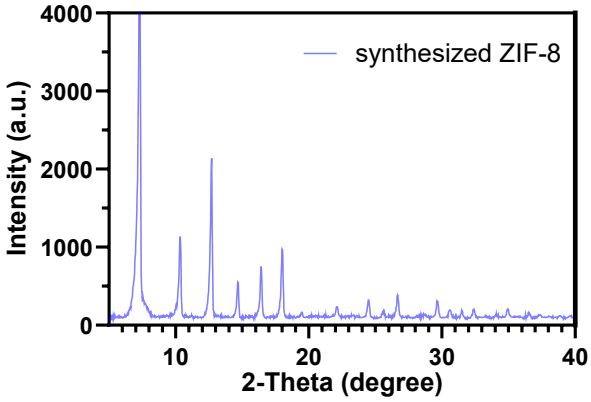

Figure S6. XRD pattern of synthesized ZIF-8.

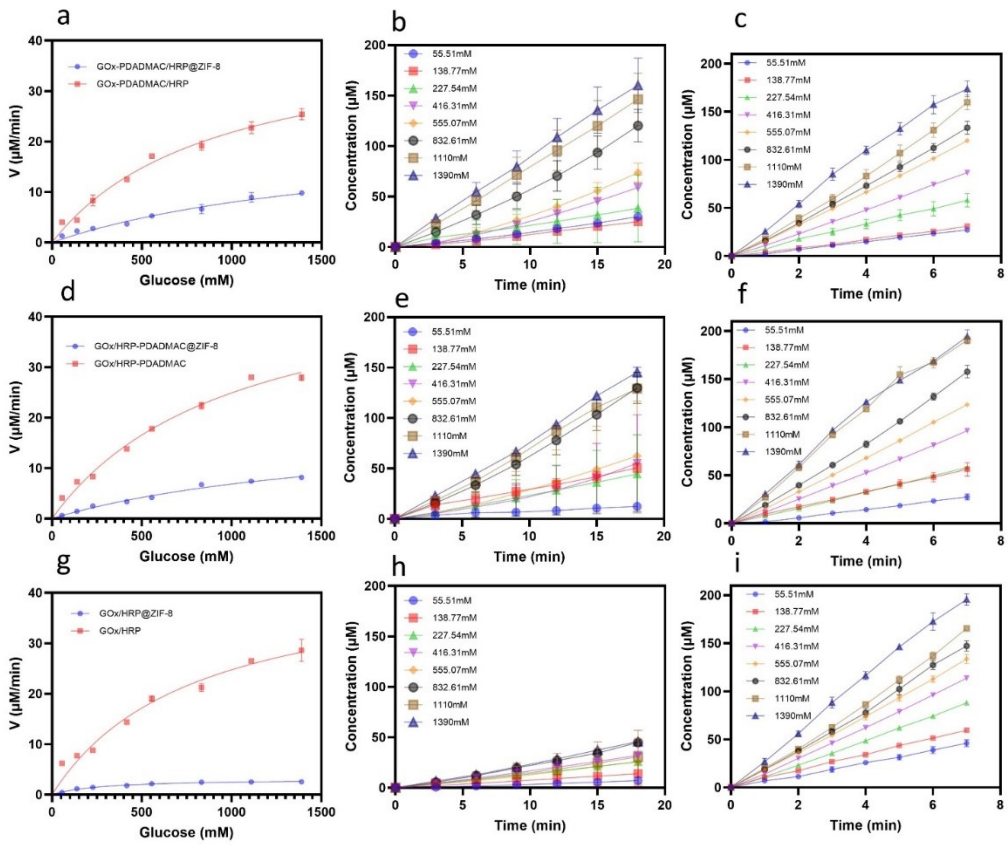

Figure S7. Comparison of enzymatic activity between enzyme-MOF samples and their free enzyme counterparts. (a) Plot of reaction velocity, V, against substrate [glucose] for GOx-PDADMAC/HRP@ZIF-8 and free GOx-PDADMAC/HRP, with (b) and (c) illustrating the DAP change over time at different glucose concentrations for GOx-PDADMAC/HRP@ZIF-8 and GOx-PDADMAC/HRP, respectively. (d) Plot of reaction velocity, V, against substrate [glucose] for GOx/HRP-PDADMAC@ZIF-8 and free GOx/HRP-PDADMAC, with (e) and (f) illustrating the DAP change over time at different glucose concentrations for GOx/HRP-PDADMAC@ZIF-8 and free GOx/HRP-PDADMAC; while (g) Plot of reaction velocity, V, against substrate [glucose] for GOx/HRP@ZIF-8 and free GOx/HRP, with (h) and (i) illustrating the DAP change over time at different glucose concentrations for GOx/HRP@ZIF-8 and free GOx/HRP. The same amount of enzymes, based on loading efficiency, was used for the comparison.

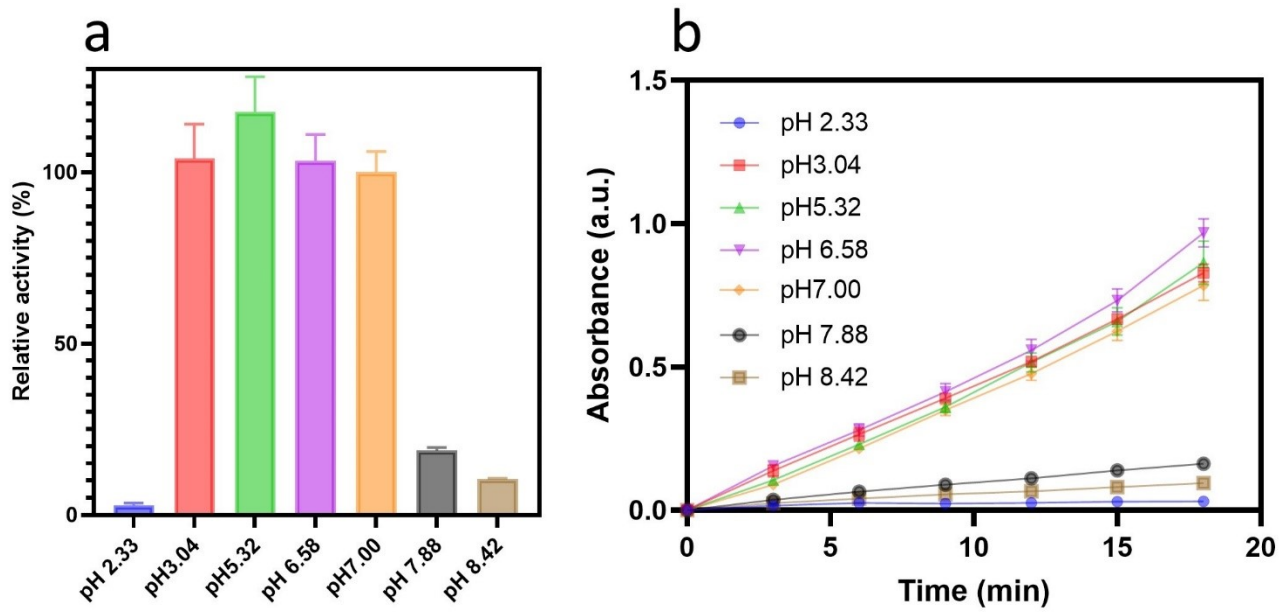

Figure S8. The catalytic activity of enzyme-MOF biocomposites across a pH range (pH 2.33 to 8.42). (a) The relative catalytic activity with neutral pH is normalized to 100%. (b)The change in absorbance over time.

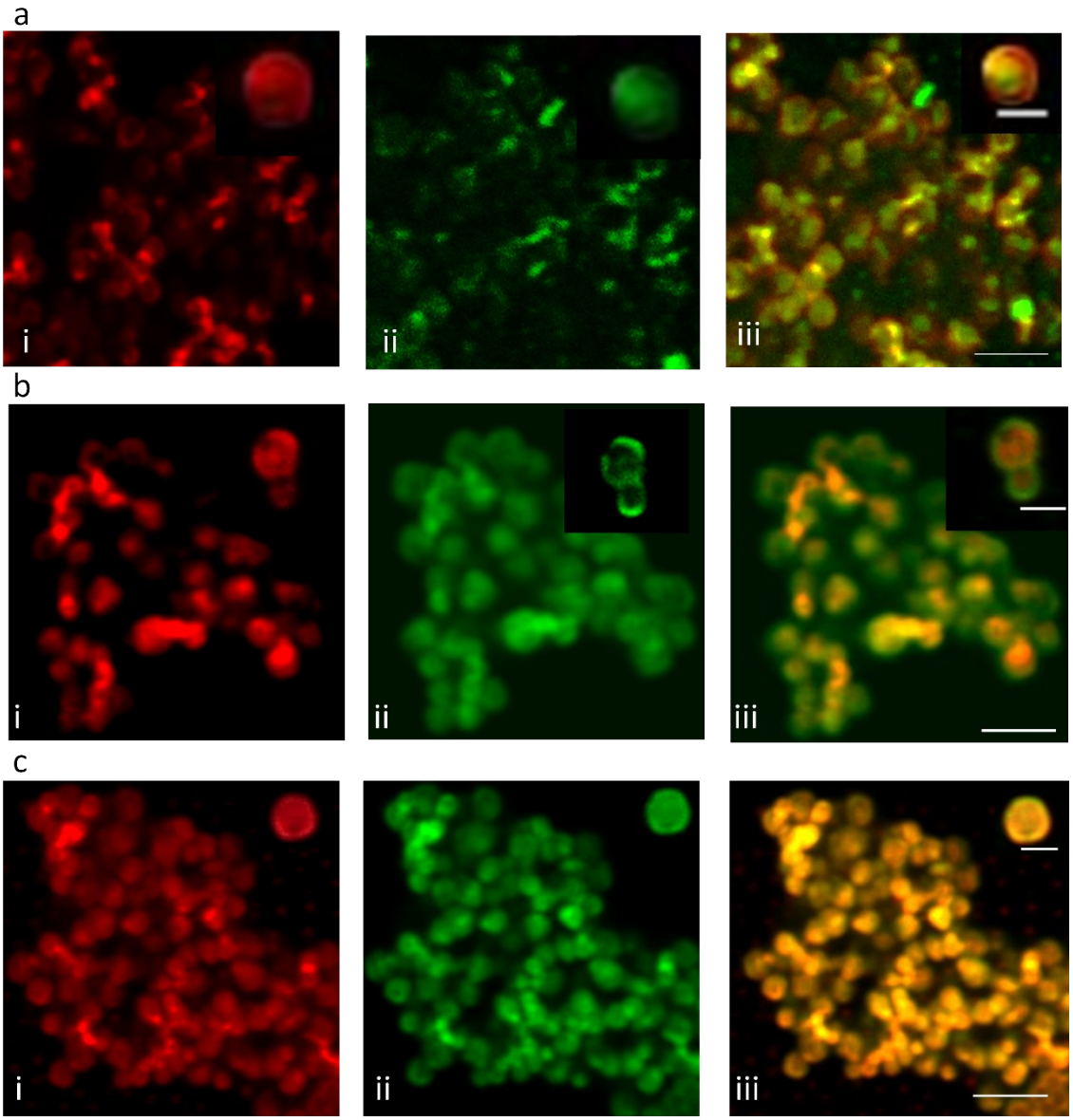

Figure S9. CLSM images of (**a**) GOx-PDADMAC/HRP@ZIF-8, (**b**) GOx/HRP-PDADMAC@ZIF-8, (**c**) GOx/HRP@ZIF-8. (i) GOx labeled with ATTO 633 (red), (ii) HRP labeled with ATTO 550 (green), and (iii) are the merged images. The scale bar in the main images is 3 μm, while the scale bar of the insets bar is 1 μm.

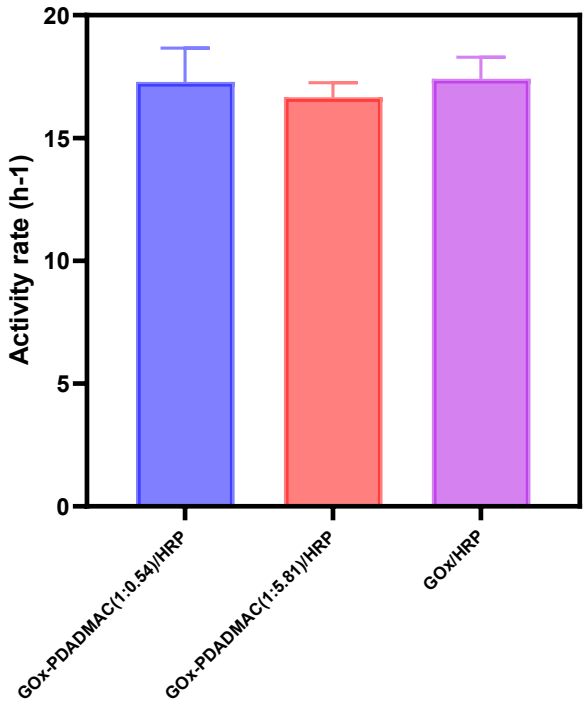

Figure S10. Calculated activity rate of GOx-PDADMAC at varying PDADMAC concentrations and free GOx enzyme according to Figure 3d.

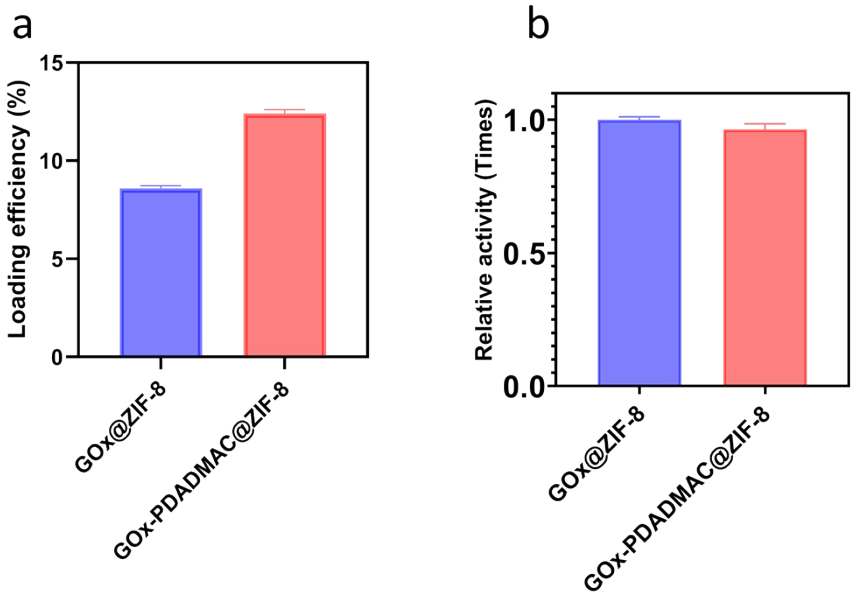

Figure S11. GOx loading efficiency in GOx@ZIF-8 and GOx@PDADMAC-ZIF-8 (**a**). Calculated enzyme activity rate of GOx@ZIF-8 and GOx-PDADMAC@ZIF-8 based on the same amount of GOx in each sample according to Figure 3e.

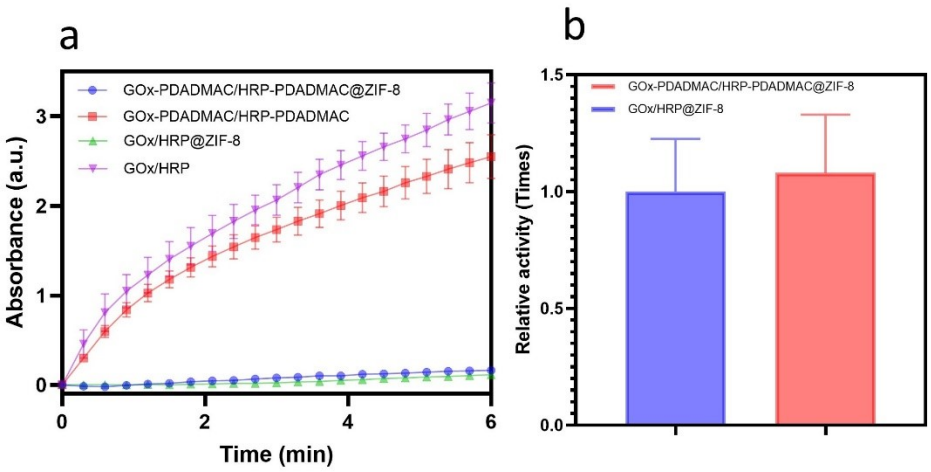

Figure S12. The comparison of enzymatic activity GOx-PDADMAC/HRP-PDADMAC@ZIF-8, GOx/HRP@ZIF-8, and their free counterparts. The same amount of enzymes, based on loading efficiency, was used for the comparison. (a) Time-dependent absorbance measurements for each sample. (b) Relative activity comparison between the modified and unmodified enzyme-MOFs.

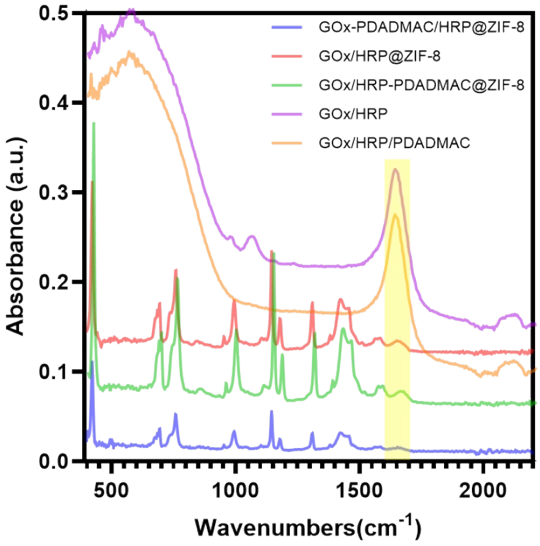

Figure S13. FTIR spectra of GOx-PDADMAC/HRP@ZIF-8, GOx/HRP-PDADMAC@ZIF-8, GOx/HRP@ZIF-8, GOx/HRP and GOx/HRP/PDADMAC. Amide I regions (1600-1700 cm^{-1}) were used to analyze their tertiary structure.

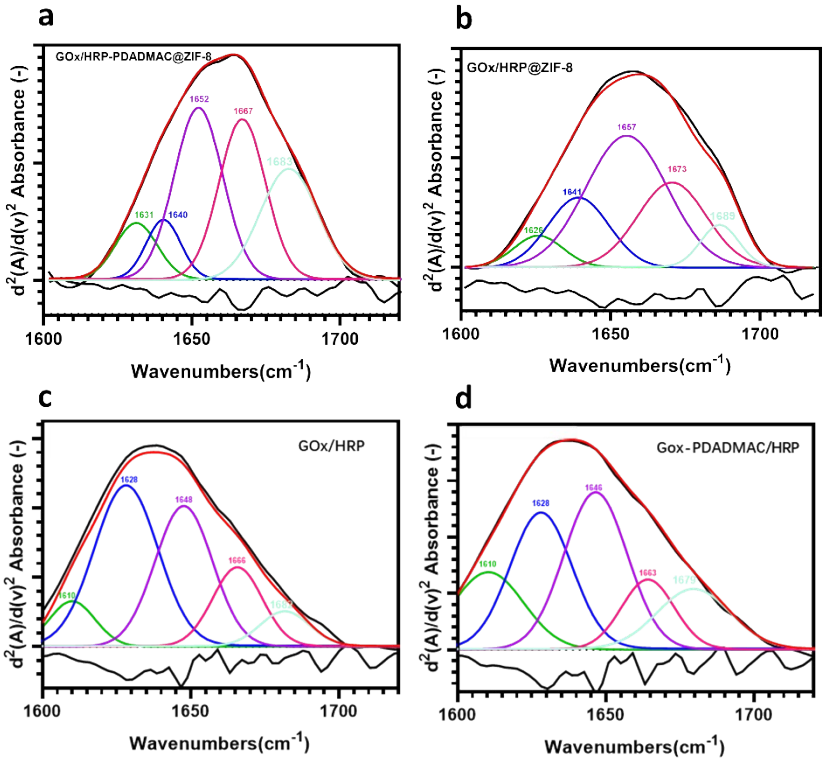

Figure S14. Deconvoluted FTIR spectra of the Amide I region (1600-1700 cm^{-1}) for GOx/HRP-PDADMAC@ZIF-8 (**a**), GOx/HRP@ZIF-8 (**b**), GOx/HRP (**c**), GOx-PDADMAC/HRP (**d**). The red line represents the simulated fit, the black line indicates the baseline-corrected experimental spectra and the lower black line shows the second derivative of the spectra.

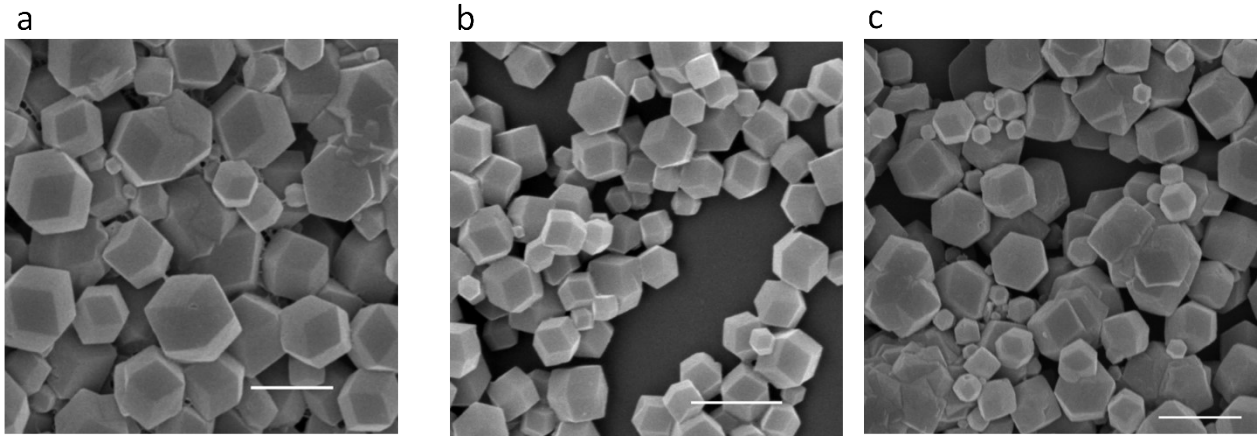

Figure S15. SEM images of as-synthesized Pro/GOx-PDADMAC@ZIF-8 **(a)**, Pro-PDADMAC/GOx@ZIF-8 (molar ratio of Pro to PDADMAC is 1: 1.13) **(b)**, Pro/GOx@ZIF-8 **(c).** The scale bar in the main images is 1 μm.

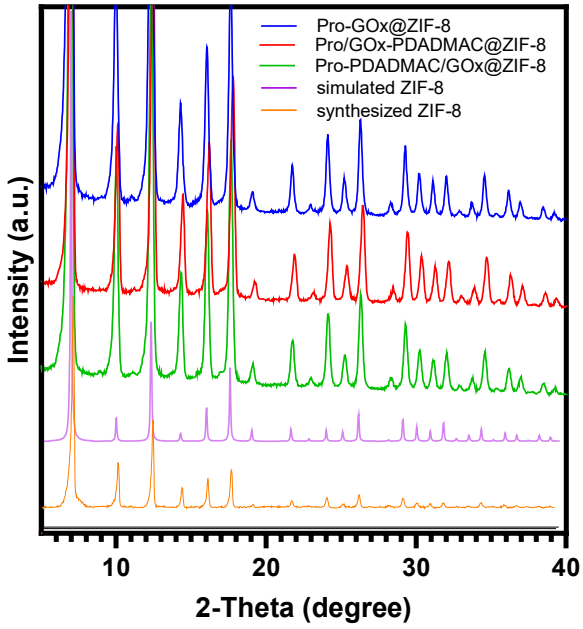

Figure S16. XRD patterns of simulated ZIF-8, synthesized ZIF-8, GOx/Pro@ZIF-8, Pro-PDADMAC/GOx@ZIF-8 and Pro/GOx-PDADMAC@ZIF-8.

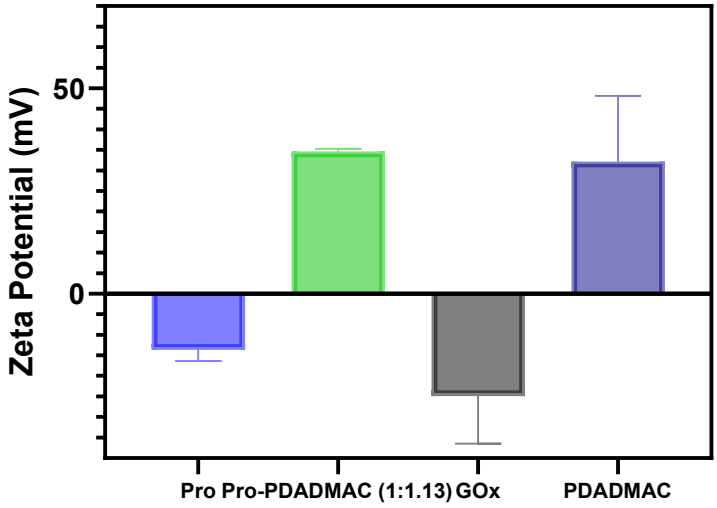

Figure S17. Zeta potential analysis of Pro and GOx modified with PDADMAC at various molar ratios

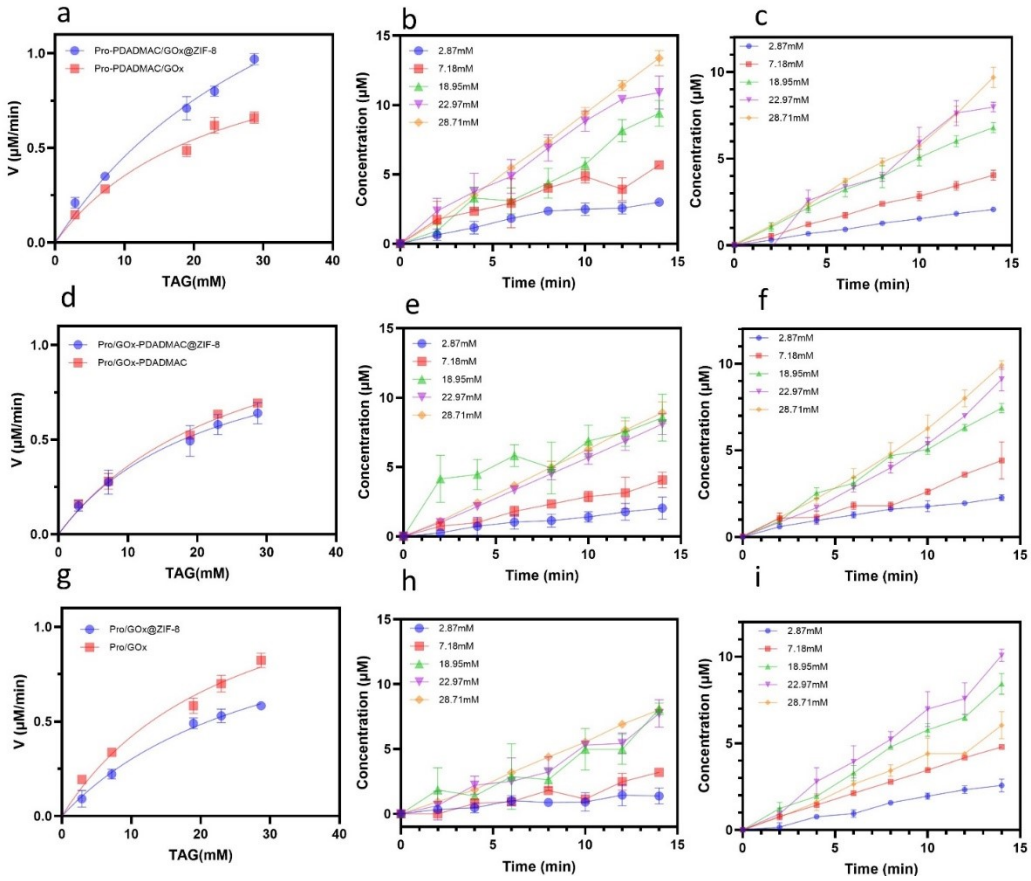

Figure S18. Comparison of enzymatic activity between enzyme-MOF samples and their free enzyme counterparts. (a) Plot of reaction velocity, V, against substrate [1,2,3,4-Tetra-O-acetyl-beta-D-glucopyranose] for Pro-PDADMAC/GOx@ZIF-8 and free Pro-PDADMAC/GOx, with (b) and (c) illustrating the DAP change over time at different substrate concentrations for Pro-PDADMAC/GOx@ZIF-8 and Pro-PDADMAC/GOx, respectively. (d) Plot of reaction velocity, V, against substrate [1,2,3,4-Tetra-O-acetyl-beta-D-glucopyranose] for Pro/GOx-PDADMAC@ZIF-8 and free Pro/GOx-PDADMAC, with (e) and (f) illustrating the DAP change in over time at different concentrations for Pro/GOx-PDADMAC@ZIF-8 and free Pro/GOx-PDADMAC; while (g) Plot of reaction velocity, V, against substrate [1,2,3,4-Tetra-O-acetyl-beta-D-glucopyranose] for Pro/GOx@ZIF-8 and free Pro/GOx, with (h) and (i) illustrating the DAP change over time at different concentrations for Pro/GOx@ZIF-8 and free Pro/GOx.

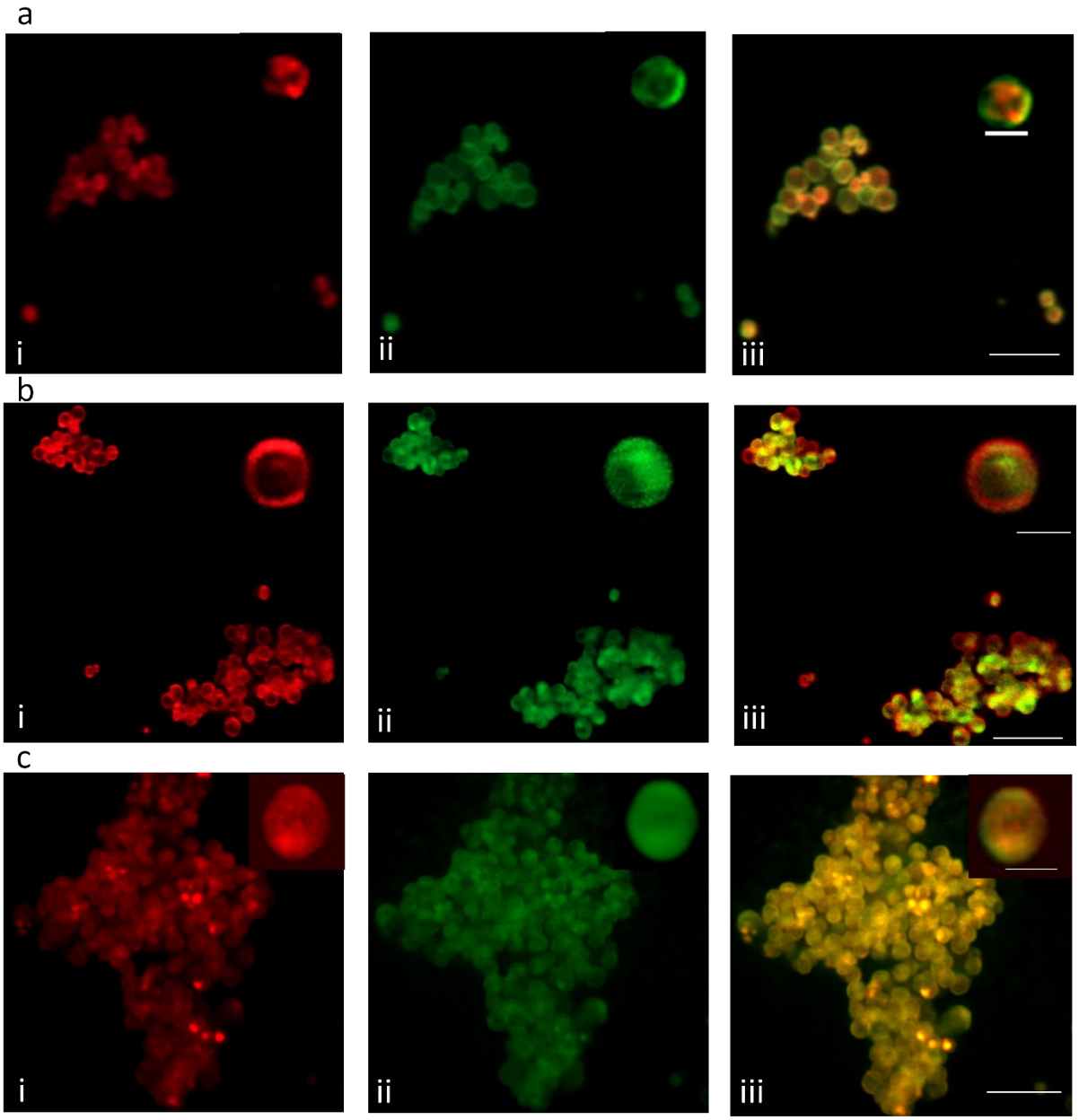

Figure S19. CLSM images of (**a**) Pro-PDADMAC/GOx@ZIF-8, (**b**) Pro/GOx-PDADMAC@ZIF-8, (**c**) Pro/GOx @ZIF-8. (i) GOx labeled with ATTO 633 (red), (ii) Pro labeled with ATTO 550 (green), and (iii) are the merged images. The scale bar in the main images is 5 μm, while the scale bar of the insets bar is 500 nm.

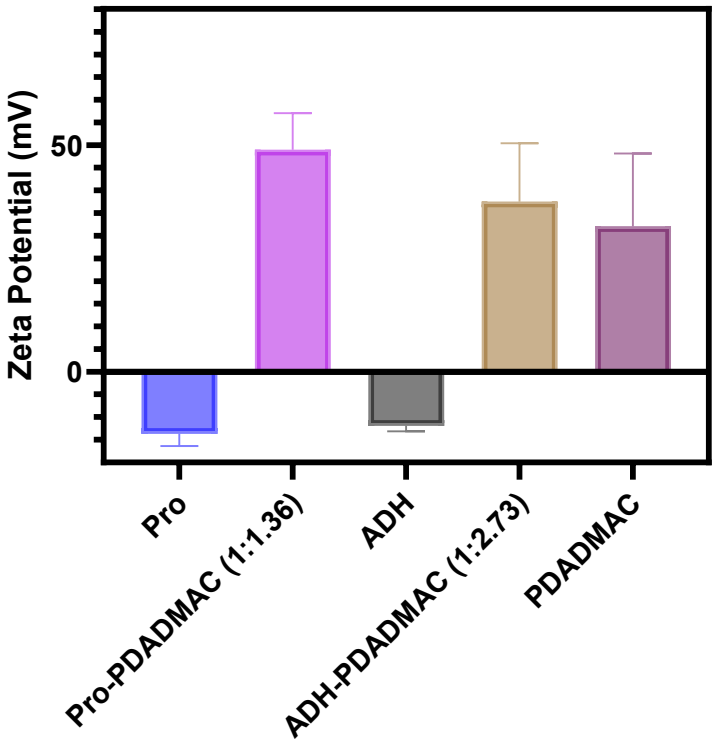

Figure S20. Zeta potential of ADH and Pro modified with PDADMAC at different molar ratios.

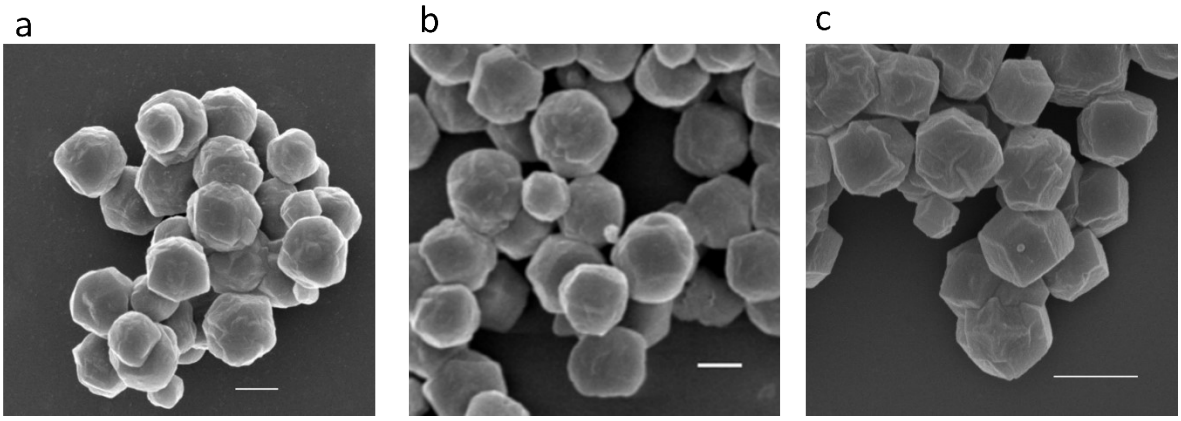

Figure S21. SEM images of as-synthesized Pro/ADH-PDADMAC@ZIF-8 **(a)** Pro-PDADMAC/ADH@ZIF-8 (molar ratio of Pro to PDADMAC is 1: 1.36); **(b)** Pro/ADH-PDADMAC @ZIF-8 (molar ratio of ADH to PDADMAC is 1: 12.73); **(c)** Pro-ADH@ZIF-8**.** The scale bar in the main images is 1 μm.

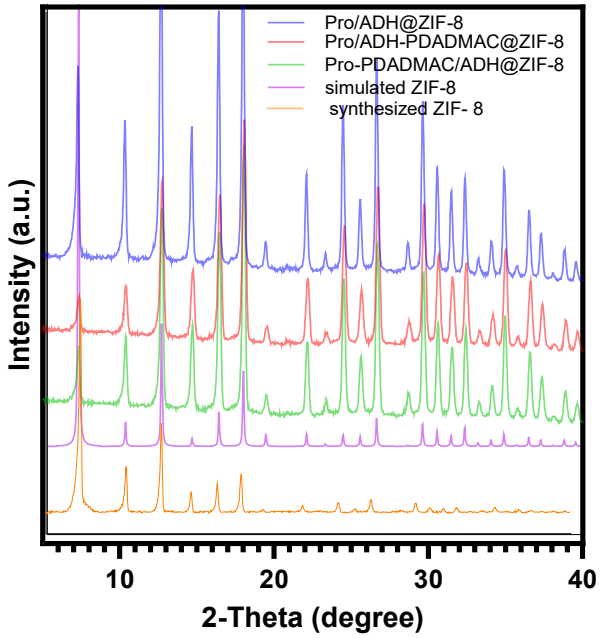

Figure S22. XRD patterns of simulated ZIF-8, synthesized ZIF-8, Pro/ADH@ZIF-8, Pro-PDADMAC/ADH@ZIF-8 and Pro/ADH-PDADMAC@ZIF-8.

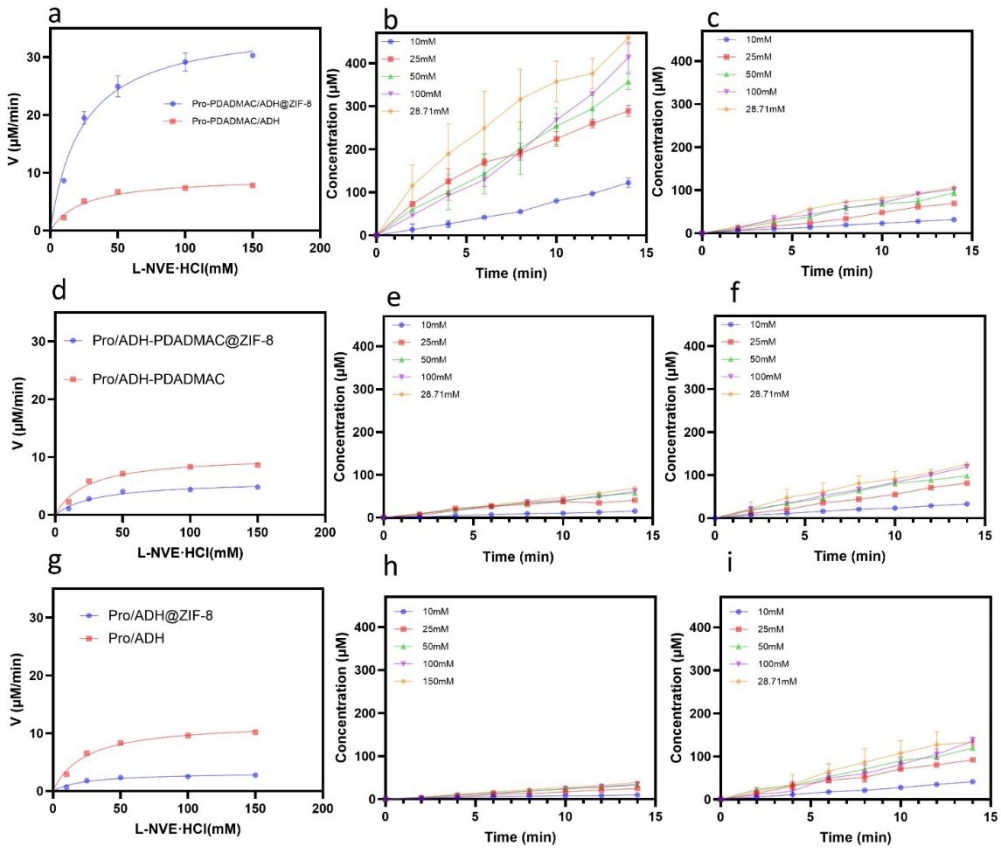

Figure S23. Comparison of enzymatic activity between enzyme-MOF samples and their free enzyme counterparts. (a) Plot of reaction velocity, V, against substrate [L-Norvaline Ethyl Ester] for Pro-PDADMAC/ADH@ZIF-8 and free Pro-PDADMAC/ADH, with (b) and (c) illustrating the NADH change over time at different substrate concentrations for Pro-PDADMAC/ADH@ZIF-8 and Pro-PDADMAC/ADH, respectively. (d) Plot of reaction velocity, V, against substrate [L-Norvaline Ethyl Ester] for Pro/ADH-PDADMAC@ZIF-8 and free Pro/ADH-PDADMAC, with (e) and (f) illustrating the NADH change over time at different substrate concentrations for Pro/ADH-PDADMAC@ZIF-8 and free Pro/ADH-PDADMAC; while (g) Plot of reaction velocity, V, against substrate [L-Norvaline Ethyl Ester] for Pro/ADH@ZIF-8 and free Pro/ADH, with (h) and (i) illustrating the NADH change over time at different substrate concentrations for Pro/ADH@ZIF-8 and free Pro/ADH.

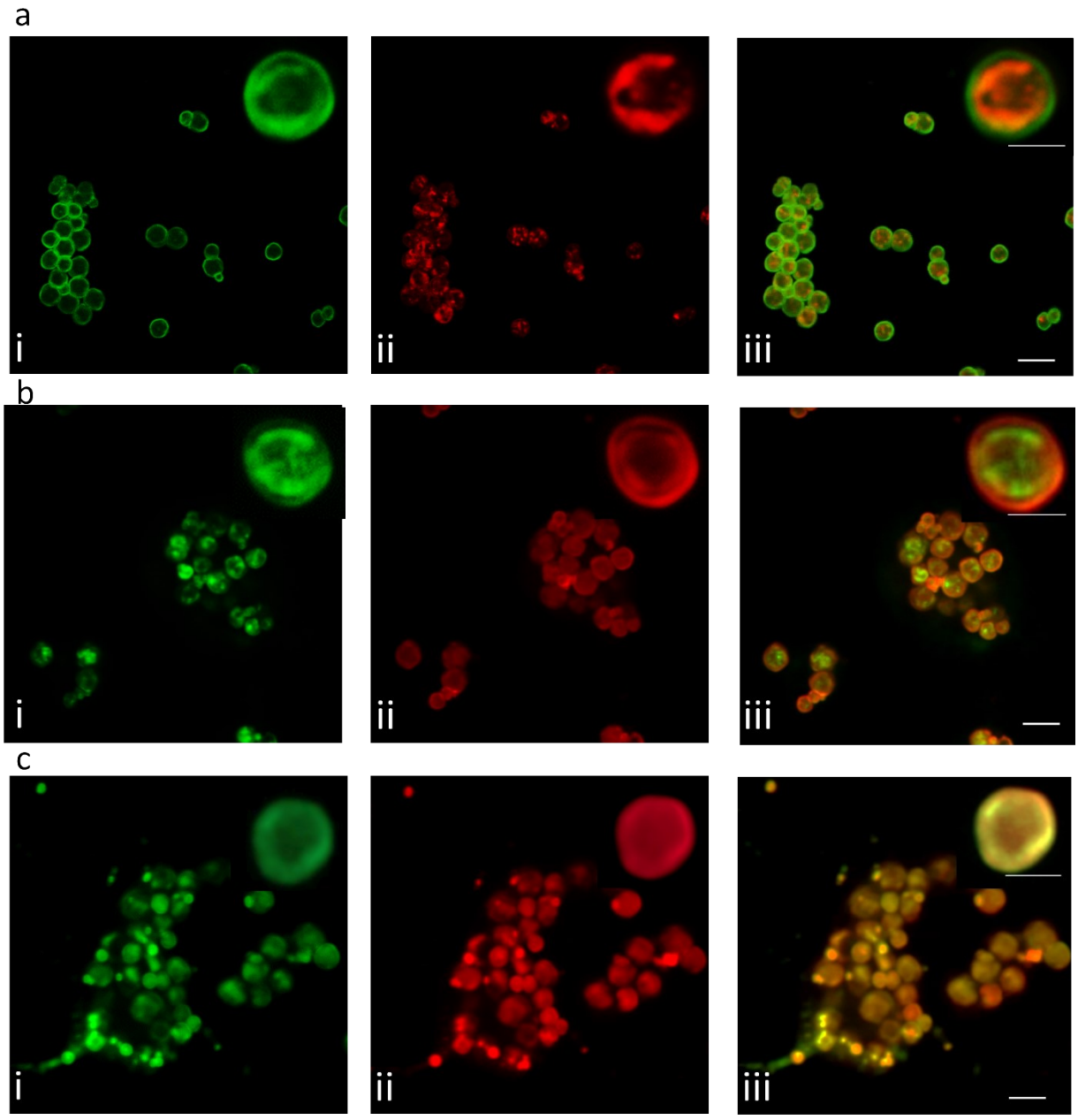

Figure S24. CLSM images of (**a**) Pro-PDADMAC/ADH@ZIF-8; (**b**) Pro/ADH-PDADMAC@ZIF-8; (**c**) Pro/ADH@ZIF-8. (i) ADH labeled with ATTO 633 (red), (ii) Pro labeled with ATTO 550 (green), and (iii) are the merged images. The scale bar in the main images is 3 μm, while the scale bar of the insets bar is 500 nm.

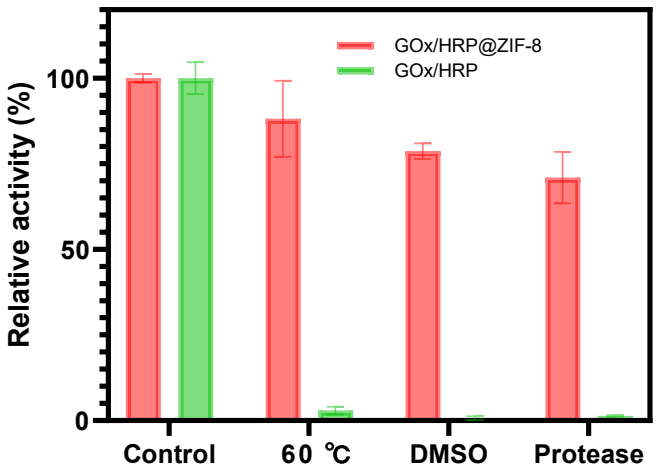

Figure S25. Relative enzymatic activities of GOx/HRP@ZIF-8, and free GOx/HRP enzymes under different stress conditions: exposure to 60°C for 1 hour, DMSO for 1 hour, and protease (0.2 mM) treatment for 2 hour.

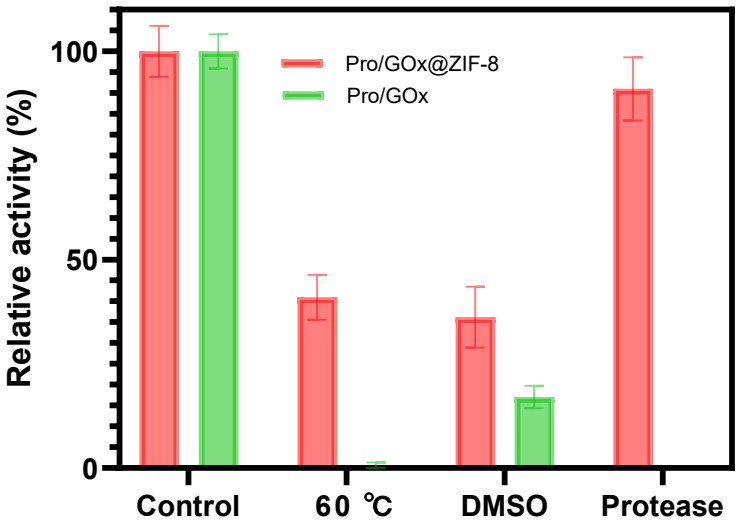

Figure S26. Relative enzymatic activities of Pro/GO@ZIF-8, and free GOx/Pro enzymes under different stress conditions: exposure to 60°C for 1 hour, DMSO for 1 hour, and protease (0.2 mM) treatment for 2 hours.

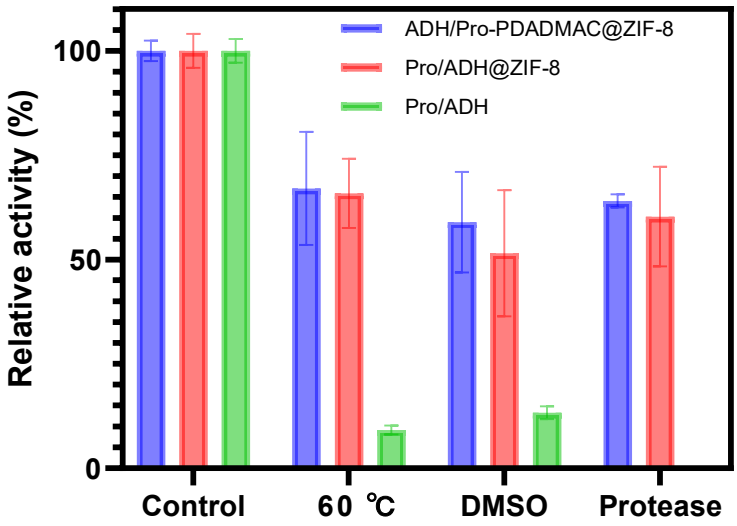

Figure S27. Relative enzymatic activities of Pro-PDADMAC/ADH@ZIF-8, Pro/ADH@ZIF-8, and free Pro/ADH enzymes under different stress conditions: exposure to 60°C for 1 hour, DMSO for 1 hour, and protease (0.2 mM) treatment for 2 hours.

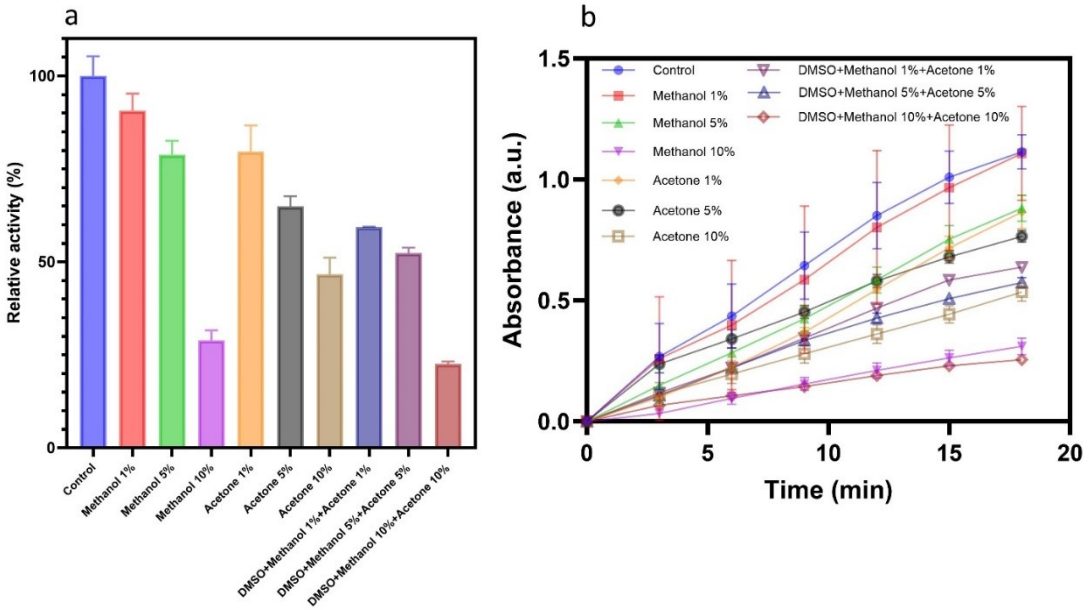

Figure S28. The catalytic activity of enzyme-MOF biocomposites in various organic solvents. (a) The relative catalytic activity. (b) The time-dependent absorbance changes across different conditions.

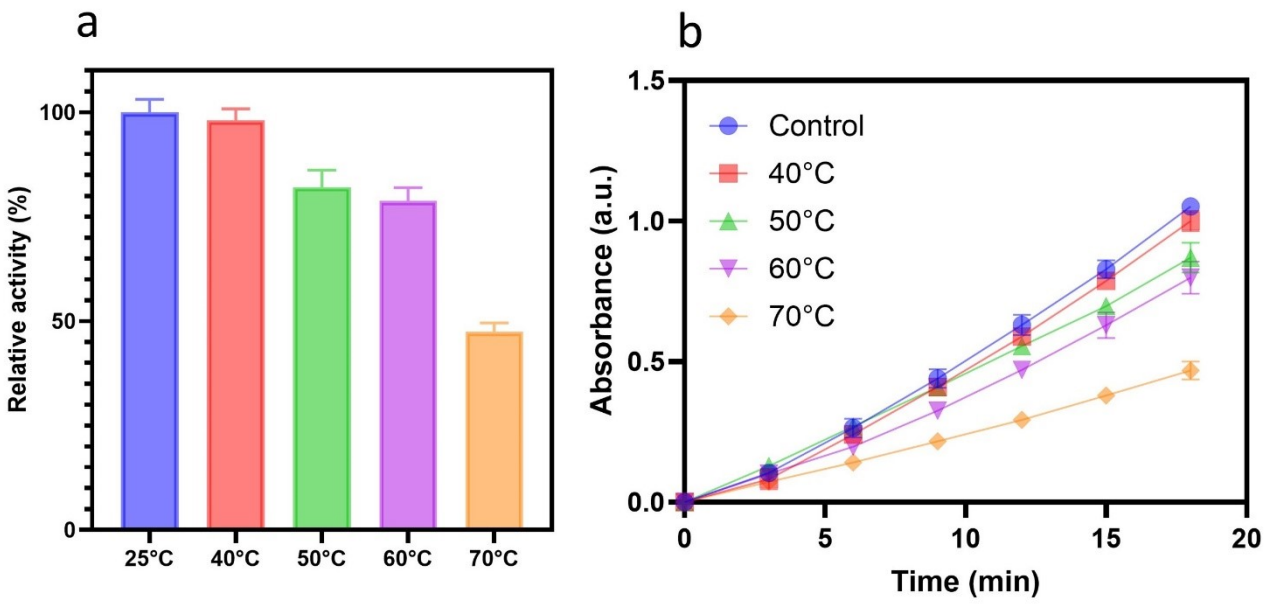

Figure S29. Thermal stability of GOx-PDADMAC/HRP@ZIF-8 at different temperatures. (a) Relative activity after incubation for one hour at 25 °C, 40 °C, 50 °C, 60 °C, and 70 °C. (b) Time-dependent absorbance at 420 nm for different temperature conditionS.

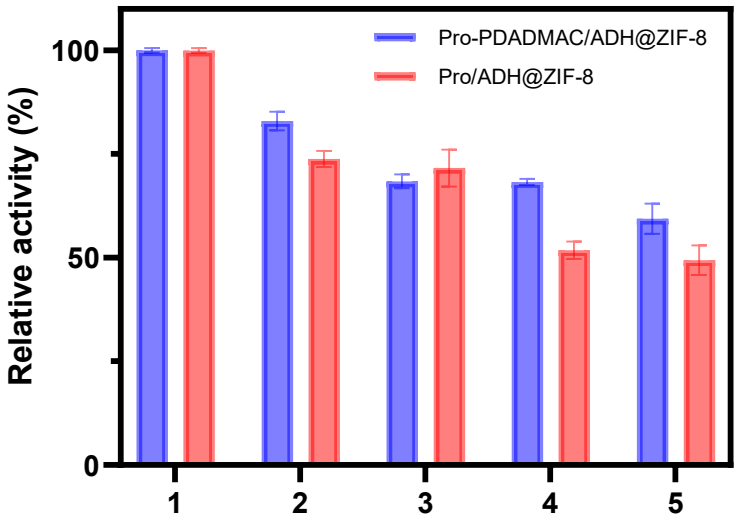

Figure S30. Relative activity of Pro-PDADMAC/ADH@ZIF-8 and Pro/ADH@ZIF-8 of catalytic reusability in five consecutive cycles.

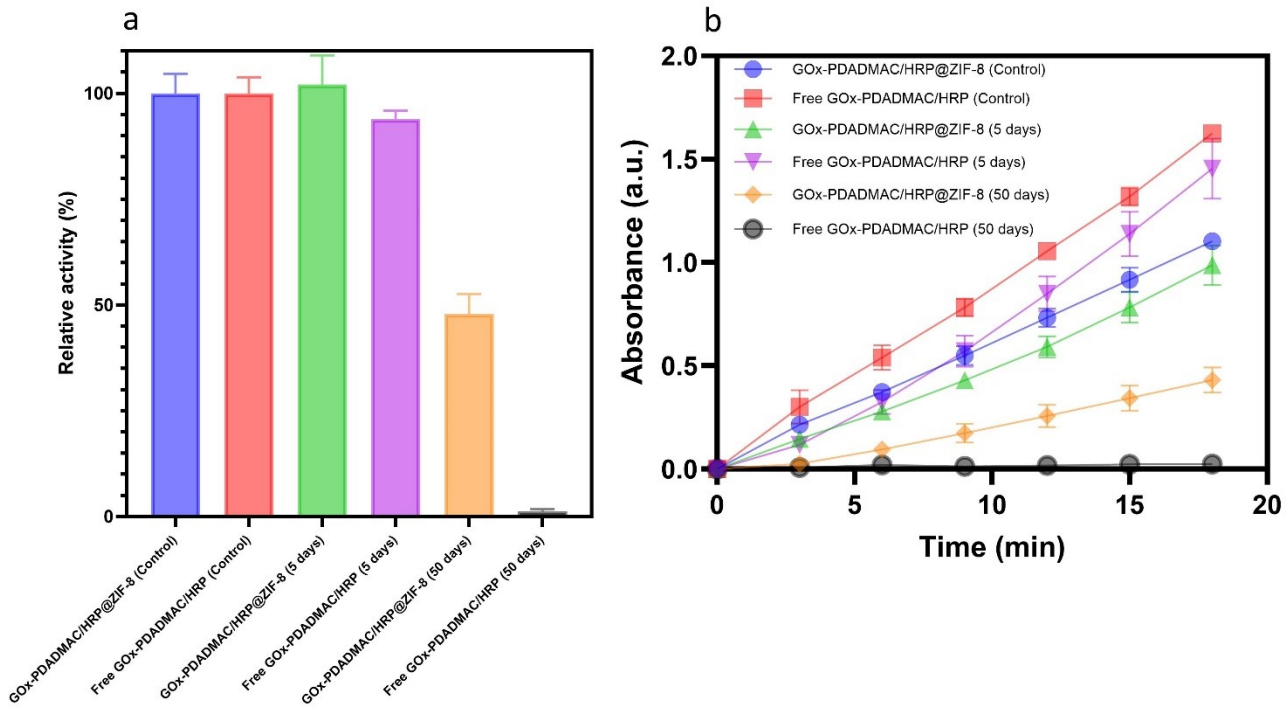

Figure S31. The long-term stability of enzyme-MOF biocomposites stored at 4 °C for 5 days and 50 days. (a) Their relative catalytic activity. (b) The change in absorbance over time at different storage durations.

Reference

1. Z. Xu, G. Xiao, H. Li, Y. Shen, J. Zhang, T. Pan, X. Chen, B. Zheng, J. Wu and S. Li, *Adv. Funct. Mater.*, 2018, **28**, 1802479.
2. T. Man, C. Xu, X.-Y. Liu, D. Li, C.-K. Tsung, H. Pei, Y. Wan and L. Li, *Nat. Commun.*, 2022, **13**, 305.
3. J. Liang, F. Mazur, C. Tang, X. Ning, R. Chandrawati and K. Liang, *Chem. Sci.*, 2019, **10**, 7852-7858.
4. C. Hu, Y. Bai, M. Hou, Y. Wang, L. Wang, X. Cao, C.-W. Chan, H. Sun, W. Li and J. Ge, *Sci. Adv.*, 2020, **6**, eaax5785.
5. Q. Wang, M. Chen, C. Xiong, X. Zhu, C. Chen, F. Zhou, Y. Dong, Y. Wang, J. Xu and Y. Li, *Biosens. Bioelectron.*, 2022, **196**, 113695.
6. J. Liang, S. Gao, J. Liu, M. Y. B. Zulkifli, J. Xu, J. Scott, V. Chen, J. Shi, A. Rawal and K. Liang, *Angew. Chem. Int. Ed.*, 2021, **60**, 5421-5428.